AN ALGORITHM FOR TRANSFORMATION OF ENERGY AND CHARGE DEPOSITION PROFILES BETWEEN NORMALLY INCIDENT AND ISOTROPICALLY INCIDENT ELECTRONS USING MONTE CARLO SIMULATIONS

David A. Barton[(1)], Brian P. Beecken[(2)]

[(1)]Air Force Research Laboratory, 3550 Aberdeen Ave. SE Kirtland AFB, NM 87107 USA, Email:david.barton.14@us.af.mil
[(2)]Physics Department, Bethel University, St. Paul, MN 55112 USA, Email:beebri@bethel.edu

ABSTRACT

Monte Carlo simulations utilizing the MCNP6 transport code have been made for electrons incident onto a Kapton slab with energies between 25 keV and 2.5 MeV. The resulting energy and charge deposition profiles for both normal and isotropic incidence were compared and an algorithm for transforming these profiles between normal and isotropic incidence was developed. The algorithm was tested and produced isotropic profiles from beam profiles that agreed to within 10% of simulated Monte Carlo profiles. Such an algorithm will allow for quick reproduction of realistic space-like electron environment charging profiles from laboratory results which primarily use electron beams.

1. INTRODUCTION

At the most fundamental level, understanding the deep-dielectric charging that occurs in spacecraft dielectrics requires knowledge of where high-energy incident electrons deposit their energy and charge. Deposition profiles, particularly of energy, have been discussed in the literature for a long time. The most widely used energy deposition algorithm dates to 1974 [1], but was updated in 1998 [2]. That energy algorithm was improved and extended in 2008 [3]. Work on charge deposition has proceeded more slowly, with the first algorithms being produced in 1994 [4] and 1995 [5]. Recently, significant work [6] has been done on refining these algorithms for the purpose of writing codes such as NUMIT [6] [7] [8], which model deep-dielectric charging.

Unfortunately, virtually all the algorithms to date have been developed for normal incidence. Therefore, because isotropic incidence more closely approximates the complex space environment, modelers of deep-dielectric charging and the resulting transport of charge within the dielectric have attempted to adapt these algorithms for normal electron-beam incidence to the case of isotropic electron incidence (e.g., [8]). Only recently [9] [10] have efforts been made to develop an algorithm based on Monte Carlo simulations that is explicitly designed for isotropic electron incidence.

In recent years, there has been a focus on experimentally determining deposition profiles by the use of Pulsed Electro-Acoustics (PEA). Some examples are [11] [12] [13] [14], and the work is ongoing. Such experiments, however, rely on normal electron beam incidence. Without a method of translating the results of such experiments to an electron incidence that more closely approximates the realistic space environment, the value of these experimental results will be limited.

Based on a very small set of Monte Carlo simulations, Frederickson and Brautigam [15] noticed that it is possible, at least for limited cases, to approximate isotropic deposition profiles by finding appropriate ratios between normal beam incidence and isotropic incidence deposition profiles. Davis et al. have utilized this method [16] in the limited case explored by Frederickson and Brautigam. We have explored further cases, particularly for Kapton, over a large range of incident energies. It appears that the ratio approach has significant merit. It could provide a pathway for applying experimentally determined depth profiles to a better understanding of spacecraft charging.

2. ALGORITHM FOR ENERGY DEPOSITION

MCNP6 Monte Carlo simulations of electron deposition into a thick Kapton slab were run for mono-energetic beams and point sources at various energies from 25 keV to 2.5 MeV. The point sources approximate isotropic incidence in space-like conditions as shown by Barton et al. [9] Once the simulations were run the profiles for both energy and charge deposited into layers of equal thickness were obtained for each incident energy and compared. The deposition profiles for the two source types had very similar proportions at the different energies, see Figs. 1 and 2.

This similarity in relative profiles across incident energies suggests that a simple relationship might be found between the two types of profiles. Such an algorithm would allow rapid creation of an isotropic profile from a beam profile or vice versa, without using experimental data or lengthy Monte Carlo simulations.

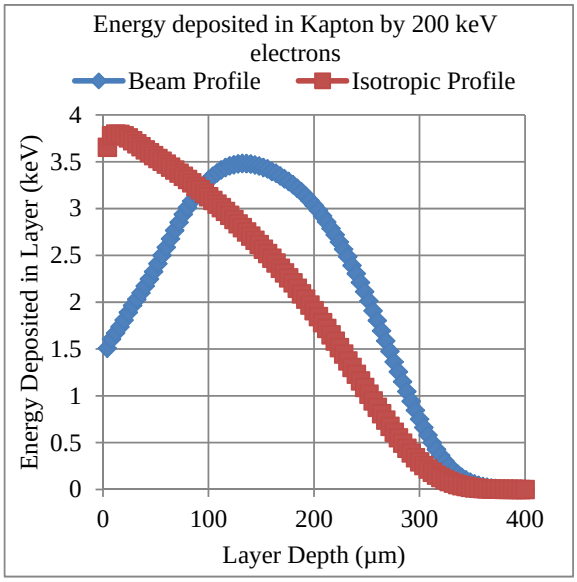

Figure 1: Electron energy deposition profile, 200 keV

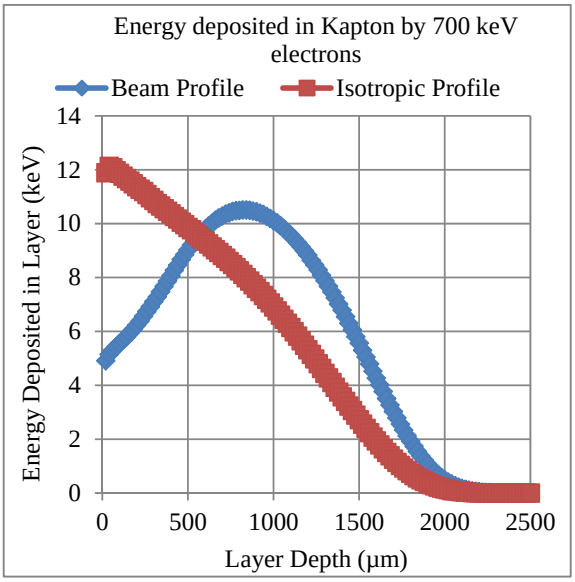

Figure 2: Electron energy deposition profile, 700 keV

To develop the algorithm, the ratio of the energies deposited for each profile was tabulated for depths equal to evenly spaced fractions of the peak energy deposition depth of the beam profile. Then these ratios were compared across the different simulated energies.

From Fig. 3 we can see two distinct groupings; a low-energy grouping of the 100 keV and lower-energy simulations, and a tighter grouping of the simulations at 200 keV and above.

The "noise" in the portion of the profile ratios above 200% depth we believe is due to the granularity of the simulation in the tails and is excluded from the calculations going forward. However, it is interesting to note that [15] showed a similar result in the tail for deposition in aluminum.

With the knowledge gained by examining the profiles we can obtain an average ratio and use that to predict an isotropic profile from a beam profile. For the average ratio we will combine the energies 200 keV and above and use a separate average for the ratios below 200 keV.

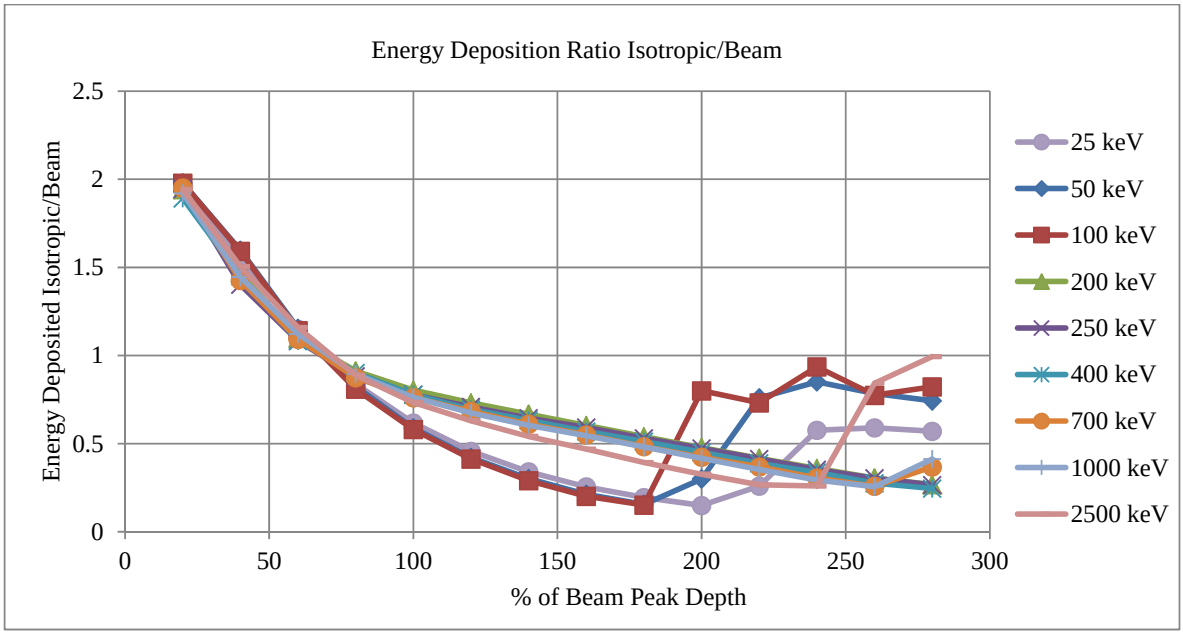

Figure 3: Energy Deposition Profile Ratios

TABLE 1: AVERAGE ENERGY PROFILE RATIOS

Position (% of Peak)	Average Ratio (E => 200 keV)	Average Ratio (E < 200 keV)
20	1.9299	1.9886
40	1.4380	1.5512
60	1.0961	1.1395
80	0.8930	0.8269
100	0.7763	0.6180
120	0.6982	0.4651
140	0.6318	0.3458
160	0.5716	0.2590
180	0.5091	0.1999
200	0.4481	0.1705
220	0.3877	
240	0.3293	
260	0.2795	
280	0.2592	

Using the averages from Tab. 1 we can now predict an energy profile for an isotropic source from a beam profile. In Figs. 4 and 5 we have done this for beam energies of 500 and 1500 keV. Then actual MC simulations were run for the isotropic cases and compared to the predictions.

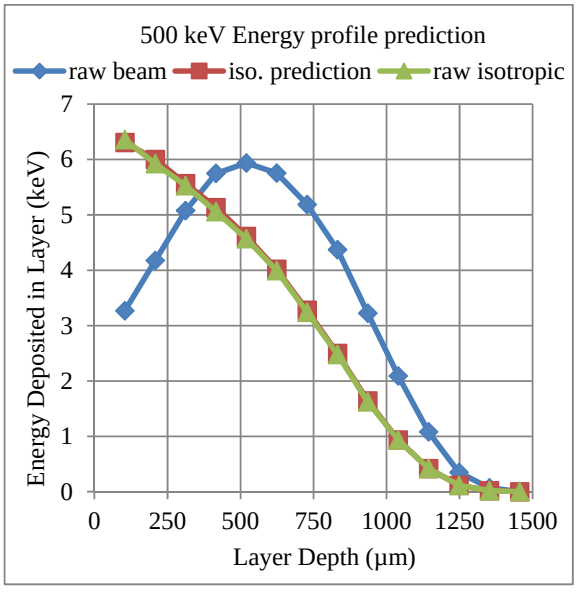

Figure 4: Energy profiles for 500 keV

As seen in Figs. 4 and 5 there is remarkably good agreement between the predicted results and the actual simulation, although there are slightly larger differences in the 1500 keV plot.

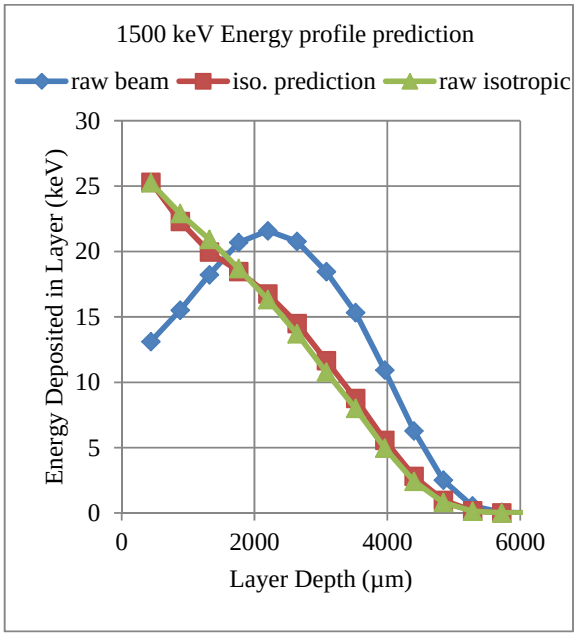

Figure 5: Energy profiles for 1500 keV

A similar prediction was made for deposition profiles at 35 keV using the low-energy average ratio. It too had very good agreement with the actual profile for the isotropic source, as seen in Fig. 6.

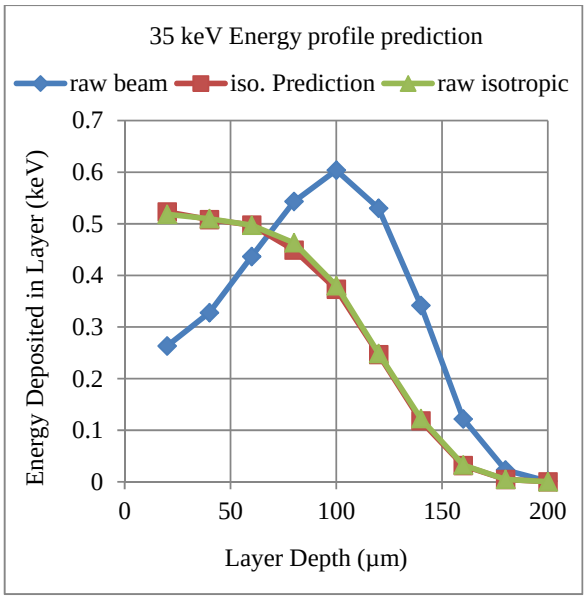

Figure 6: Energy profiles for 35 keV

3. ALGORITHM FOR CHARGE DEPOSITION

Now we graph the profiles for the charge deposited (Figs. 7 and 8), and as with the energy profiles we see similar proportions for the profiles at different energies.

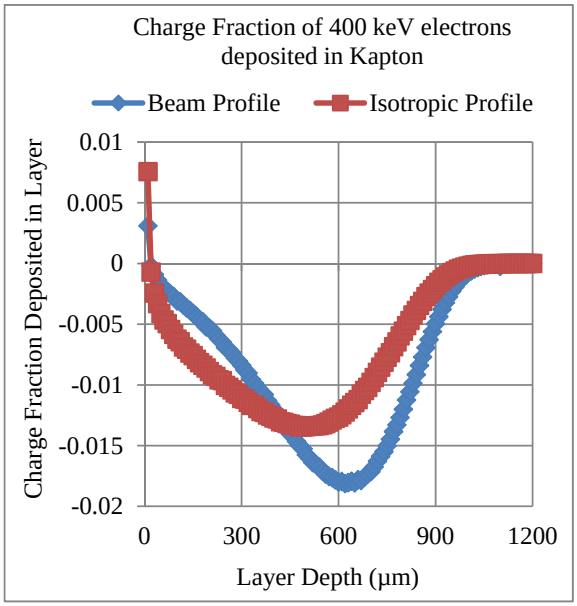

Figure 7: Charge Fraction profiles for 400 keV

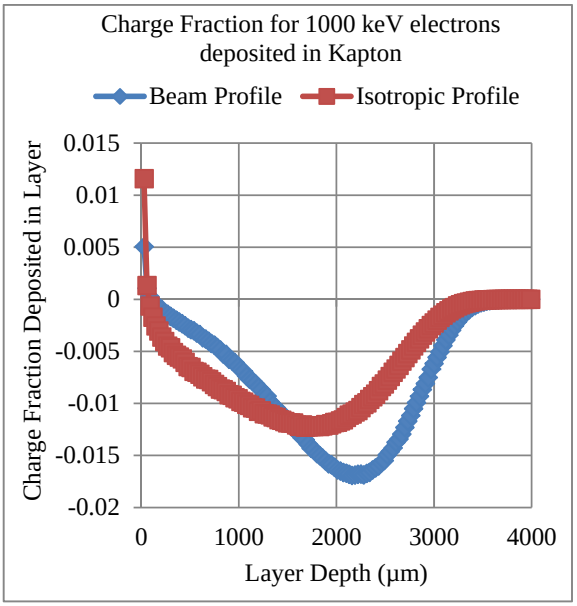

Figure 8: Charge Fraction profiles for 1000 keV

We now compare these ratios of the charge deposition profiles at different energies, but we run into a problem due to the crossover from positive to negative charging at very shallow depths. This causes instability in the ratio at these depths because of the division by numbers close to zero. To avoid this problem the charge fraction values are shifted away from zero by adding one to the profile at every point. This eliminates the instability at the shallow depths and then the ratios are compared over several energies as done previously with the energy deposition ratios (Fig. 9).

Here too there appear to be two groupings with the low energy ratios (100 keV and below) being significantly different than the high energy ratios, although the groupings are less distinct than for the energy deposition ratios. The average ratios are once again separated into high-E and low-E portions as shown in Tab. 2. Then using these average ratios we made predictions of the charge deposition profiles for isotropic incidence for 500 keV and 1500 keV incident electrons (Figs. 10 and 11).

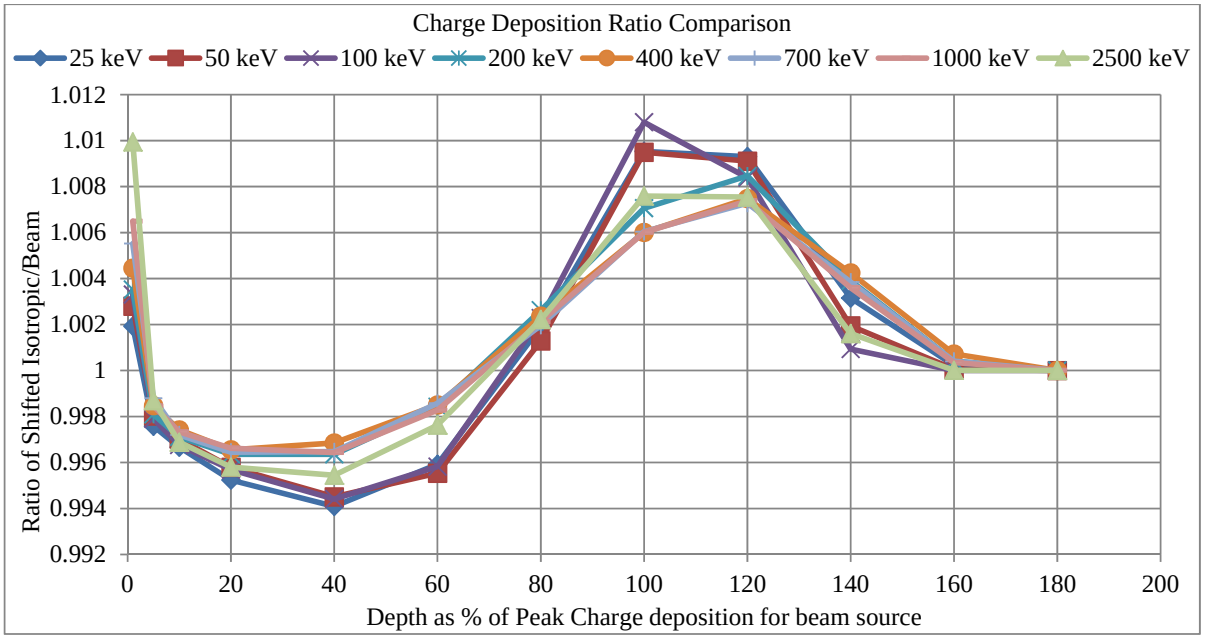

Figure 9: Charge Deposition Profile Ratios

TABLE 2: AVERAGE CHARGE FRACTION PROFILE RATIOS

% Beam Peak Depth	Average Ratio (E => 200 keV)	Average Ratio (E < 200 keV)
1	0.9941	0.9972
5	1.0015	1.0020
10	1.0028	1.0030
20	1.0037	1.0042
40	1.0037	1.0055
60	1.0017	1.0041
80	0.9977	0.9981
100	0.9935	0.9902
120	0.9924	0.9918
140	0.9966	0.9984
160	0.9996	0.9999
180	1.0000	1.0000

At 1500 keV we see very good agreement with generally less than 10% difference between the predicted and actual points (Fig. 10), however for 500 keV there is substantially more difference (Fig. 11). The peaks do not line up and on average there is about 20% difference between the prediction and the simulation. This is still fairly good agreement, but why this difference appears here is a bit of a puzzle. Examining the shifted charge profile ratios at 500 keV shows large differences from both the low-energy and high-energy average profile; however, other energies tried have closer agreement. More work needs to be done to understand the variation of the simulated charge profile from the prediction at energies near 500 keV.

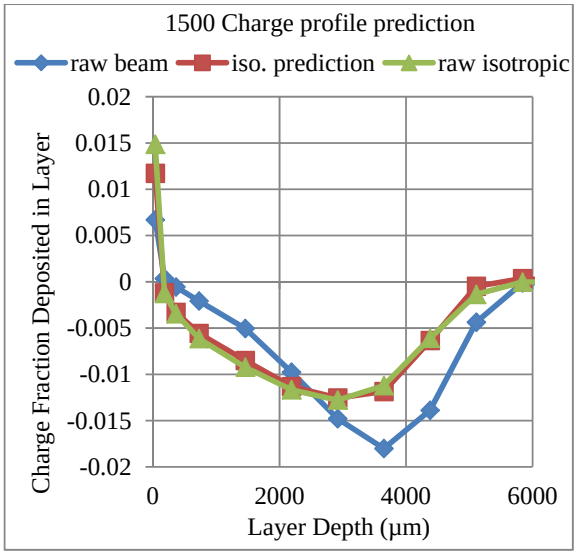

Figure 10: Charge fraction profiles for 1500 keV

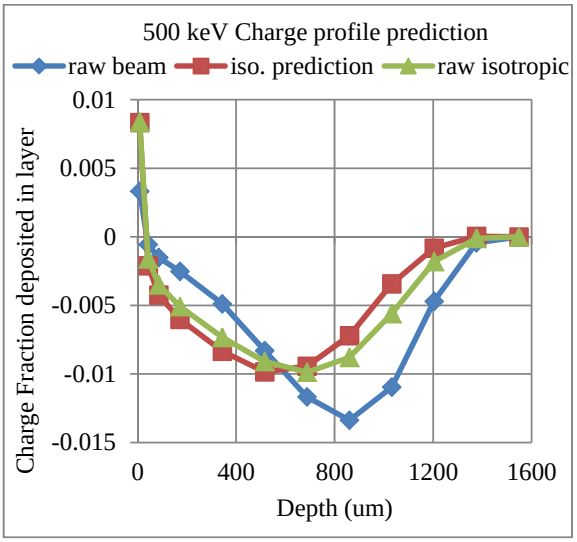

Figure 11: Charge fraction profiles for 500 keV

A prediction using the average low-energy profile was made for charge deposition from a 35 keV beam (Fig. 12). The results are quite good, with an average of about 10% difference between the prediction and the Monte Carlo simulation except for in the tail. The match between the prediction and the simulation is much better here than for the case at 500 keV, particularly in matching the peak of the profile.

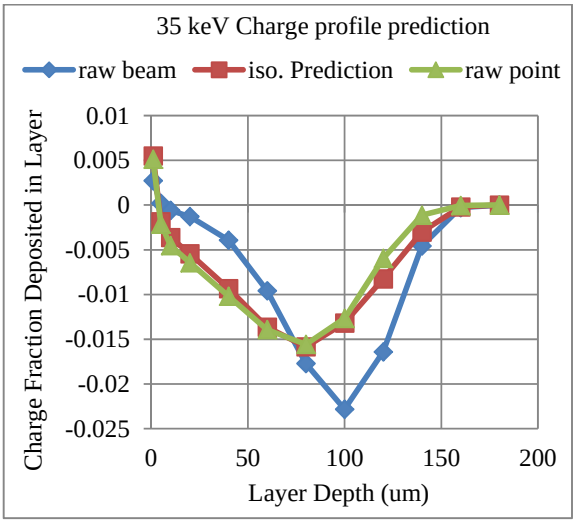

Figure 12: Charge fraction profiles for 35 keV

4. CONCLUSION

An algorithm for transforming energy and charge deposition profiles by beam sources into isotropic source profiles has been developed and works well. Predicted energy profiles are nearly the same as the actual simulation results. There is more variance in the

charge deposition profile results; nevertheless the agreement is still quite good.

Interestingly, the use of a scaling ratio works consistently within a range of lower incident energies, but a different scaling ratio is required at a higher range of energies. More work remains to be done in exploring the dependence on source particle energy and how the low-energy and high-energy algorithms connect in the region between 100 keV and 200 keV. It may be that some type of interpolation between the low-energy and high-energy ranges could be effective in improving the algorithm. The reason for two different regimes is puzzling, but there might be a clue here to the physics at work. Perhaps the cause is the compound nature of Kapton. Doing comparable work on elemental materials may either refute or provide some support for that notion depending on whether a two-regime algorithm is required.

In general, the dependence of the profiles on the target material should be explored in the future. We have performed some initial work with another material, and it looks like a similar type of algorithm could be used. If so, then the possibility arises of developing a more general algorithm that would not require Monte Carlo simulations for both beam and isotropic incidence. Such an algorithm could potentially be used to take experimental results for beam incidence and make predictions for isotropic incidence.

5. REFERENCES

1. Tabata, T. & Ito, R. (1974). An Algorithm for the Energy Deposition by Fast Electrons, Nuclear Science and Engineering. 53, 226-239.
2. Tabata, T., Andreo, P. & Shinoda, K. (1998). An algorithm for depth-dose curves of electrons fitted to Monte Carlo data, Radiation Physics and Chemistry. 53(3), 205-215.
3. Kim, W., Jun, I. & Garrett, H.B. (2008). An Algorithm for Determining Energy Deposition Profiles in Elemental Slabs by Low (< 100 keV) Energy Electrons: An Internal Charging Application. IEEE Trans. Nuc. Sci., 55(6), 3158-3163.
4. Tabata, T., Andreo, P. & Ito, R. (1994). Depth profile of charge deposition by 0.1- to 100-MeV electrons in elemental absorbers. Nucl. Instr. Meth. B, 94(1), 103-106.
5. Frederickson, A.R., Bell, J.T. & Beidl, E.A. (1995). Analytic Approximation for Charge Current and Deposition by 0.1 to 100 MeV Electrons in Thick Slabs. IEEE Trans. Nuc. Sci., 42(6), 1910-1921.
6. Kim, W., Jun, I. & Garrett, H.B. (2012). NUMIT 2.0: the latest version of the JPL internal charging analysis code. In Proc. of the 12th Spacecraft Charging Technology Conference, (CD-ROM), Kitakyushu, Japan.
7. Jun, I., Garrett, H.B., Kim, W. & Minow, J.I. (2008). Review of an Internal Charging Code, NUMIT. IEEE Trans. Plasma Sci. 36(5), 2467-2472.
8. Beecken, B.P., Englund, J.T., Lake, J.J. & Wallin, B.M. (2015). Application of AF-NUMIT2 to the Modeling of Deep-dielectric Spacecraft Charging in the space Environment, IEEE Trans. Plasma Sci. 43(9), 2817–2827.
9. Barton, D.A., Beecken, B.P. & Hoglund, R.M., (2015). Determination of Energy and Charge Deposition Profiles in Elemental Slabs From an Isotropically Equivalent Electron Source Using Monte Carlo simulations. IEEE Trans. Plasma Sci. 43(9), 2861–2868.
10. Beecken, B.P., Dirks, S.B., Gronseth, S.W. & Barton, D.A. (2016). A new algorithm for the determination of energy and charge deposition profiles in various materials resulting from isotropic electron incidence. To be published in Proc. of the 14th Spacecraft Charging Technology Conference, (CD-ROM), Noordwijk, NL.
11. Takada, T., Miyake, H. & Tanaka, Y. (2006). Pulse acoustic technology for measurement of charge distribution in dielectric materials for spacecraft. IEEE Trans. on Plasma Science 34, 2176-2184.
12. Tashima, D., Kurosawatsu, K., Sung, Y.M., Otsubo, M. & Honda, C. (2007). Spatio-temporal charge behavior in electric double layer capacitors observed by pulsed electro acoustic method. Electrochimica acta, 52, 5071-5075.
13. Bamji, S., Dakka, M.A., & Bulinski, A. (2007). Phase-resolved pulsed electro-acoustic technique to detect space charge in solid dielectrics subjected to AC voltage. IEEE Trans. on Dielectrics and Electrical Insulation, 14, 77-82.
14. Arnaout, M., Berquez, L., Baudoin, F. & Payan, D. (2010). Contribution to improving the spatial resolution of a pulsed electro acoustic cell measurement: An analysis of acoustics waves propagation. In Proc. of 10th IEEE International Conference on Solid Dielectrics (ICSD), 1-4.
15. Frederickson, A.R. & Brautigam, D.H. (2004). Mining CRRES IDM Pulse Data and CRRES Environmental Data to Improve Spacecraft Charging/Discharging Models and Guidelines. NASA/CR—2004–213228, NASA Center for AeroSpace Information, Hanover, MD, USA.
16. Davis, V.A., Mandell, M.M., & Maurer, R.H. (2007). Preliminary Surface and Internal Charging Analysis of the Radiation Belt Storm Probes Spacecraft. In Proc. of the 10th Spacecraft Charging Technology Conference, (CD-ROM), Biarritz, France.